5164 *Inorg. Chem.* **2009**, *48*, 5164–5176
DOI: 10.1021/ic900031c

Inorganic Chemistry
Article

Density-Functional Theory Study of the Stereochemistry of Chloroiron(III) and Chloromanganese(III) Complexes of a Bridled Chiroporphyrin

Latévi Max Lawson Daku,[†,*] Anna Castaings,[‡] and Jean-Claude Marchon[‡]

[†]*Département de chimie physique, Université de Genève, 30 quai Ernest-Ansermet, CH-1211 Genève 4, Switzerland, and* [‡]*Laboratoire de Chimie Inorganique et Biologique (UMR E3 CEA-UJF), Institut Nanosciences et Cryogénie, CEA Grenoble, 38054 Grenoble, France*

Received January 8, 2009

Transition metal complexes of chiroporphyrins, in which two adjacent meso substituents are linked by a strap of eight methylene groups, [M(BCP8)], can exist as either an $\alpha\alpha\alpha\alpha$ or $\alpha\beta\alpha\beta$ atropisomer depending on the nature of the coordinated metal cation. This remarkable conformational versatility was investigated by density-functional theory calculations for the d^5 chloroiron(III) complex in the low-spin and high-spin states and for the d^4 high-spin chloromanganese(III) complex. The lowest-lying electronic state of all of the conformers of the chloroiron(III) bridled chiroporphyrin is found to be the high-spin state. For the chloroiron(III) complex in the low-spin or the high-spin state and for the high-spin chloromanganese(III) complex, the most stable form is predicted to be the $\alpha\alpha\alpha\alpha$ conformer in which the chloride axial ligand is located within the cavity provided by the bridles. The predicted stereochemistries are compared with those similarly obtained (*i*) for the chloroiron(III) and chloromanganese(III) complexes of the tetramethylchiroporphyrin, which is devoid of straps, and (*ii*) for the d^{10} zinc(II) and low-spin d^8 nickel(II) BCP8 complexes, on the basis of the effects tied to the occupancy of the stereochemically active $d_{x^2-y^2}$-type antibonding orbital level, to the restraints imposed by the straps, and to the presence of the axial chloride ligand.

1. Introduction

Transition metal complexes of the bridled chiroporphyrin H_2BCP8 (BCP = bridled chiroporphyrin), in which meso substituents derived from 1(*R*)-*cis*-hemicaronaldehyde (biocartol) are connected by eight $-CH_2-$ groups (Figure 1), exhibit two drastically different conformations depending on the nature of the central metal cation.[1,2]

They can exist as an $\alpha\alpha\alpha\alpha$ or $\alpha\beta\alpha\beta$ atropisomer, where α and β refer to the location of the meso cyclopropyl substituents above (α) or below (β) the average plane of the macrocycle. Thus, the zinc(II) and low-spin (LS) nickel(II) complexes [Zn(BCP8)] (**1̂**) and [Ni(BCP8)] (**2̂**) are isolated as the $\alpha\alpha\alpha\alpha$ and $\alpha\beta\alpha\beta$ conformers, respectively.[1] [The $\alpha\alpha\alpha\alpha$ and $\alpha\beta\alpha\beta$ stereoisomers of a species rigorously are atropisomers,[3] but we will use as well the nearly equivalent term conformers for convenience (see also ref 4).] The X-ray structures of the $\alpha\alpha\alpha\alpha$-**1̂** and $\alpha\beta\alpha\beta$-**2̂** complexes are shown in Figure 2. In the open $\alpha\beta\alpha\beta$ conformation adopted by the LS nickel(II) complex (Figure 2, bottom), the porphyrim macrocycle is ruffled and the bridles connect opposite faces. In contrast, the macrocycle is slighty domed in the $\alpha\alpha\alpha\alpha$ conformation of the zinc(II) complex (Figure 2, top), and the bridles located on a same face are folded together like a pair of tweezers. While the conformational discrimination apparently is exclusive for BCP8 complexes, chiroporphyrins with longer bridles seem to be more conformationally tolerant. Thus, the chloromanganese(III) complex [MnCl(BCP10)] is obtained and isolated as a mixture of the two $\alpha\alpha\alpha\alpha$ and $\alpha\beta\alpha\beta$ conformers.[2] The possibility of achieving a fine control of the $\alpha\alpha\alpha\alpha \leftrightarrow \alpha\beta\alpha\beta$ change of conformations in complexes of BCPs is really appealing, as this would provide a route to the design of nanoscale devices such as molecular swiches or nanotweezers. This is the reason why we are investigating the conformational versatility of complexes of BCPs using both experimental and theoretical approaches.

The ability to monitor the conformations of these BCP complexes is essential to their study, especially with regard to their proposed use as nanodevices. The determination of solution conformations of organic molecules and diamagnetic

*To whom correspondence should be addressed. E-mail: max.lawson@unige.ch.

(1) Gazeau, S.; Pécaut, J.; Marchon, J.-C. *Chem. Commun.* **2001**, 1644–1645.

(2) Gazeau, S.; Pécaut, J.; Haddad, R.; Shelnutt, J. A.; Marchon, J.-C. *Eur. J. Inorg. Chem.* **2002**, 2956–2960.

(3) Eliel, E. L.; Wilen, S. H.; Mander, L. N. *Stereochemistry of Organic Compounds*; John Wiley & Sons: New York, 1994.

(4) Conformer and atroposimers are defined by Eliel et al. as follows:[3] "*Conformer* (conformational isomer): One of a set of stereoisomers that differ in conformation, that is, in torsion angle or angles. Only structures corresponding to potential energy minima (local or global) qualify." "*Atropisomers*: Stereoisomers resulting from restricted rotation about single bonds where the rotational barrier is high enough to permit isolation of the isomeric species." The $\alpha\alpha\alpha\alpha$ and $\alpha\beta\alpha\beta$ stereoisomers are atropisomers. But, for convenience, we indifferently employ the terms conformers and atropisomers, thus implying high rotational barriers.

 Published on Web 05/08/2009

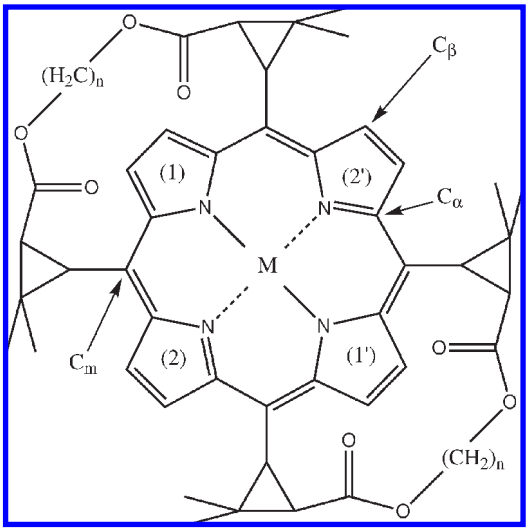

Figure 1. Structure of the bridled chiroporphyrin BCP*n* complexes. In the present study, $n = 8$. The atom labeling used is also indicated.

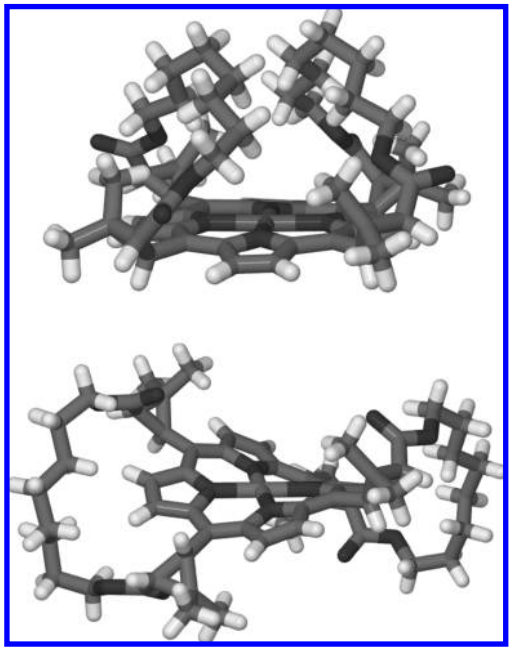

Figure 2. X-ray structures[1] of the zinc(II) αααα-**î** (top) and LS nickel(II) αβαβ-**î** (bottom) BCP8 complexes.

complexes generally is obtained by NMR spectroscopic methods. However, in the case of paramagnetic species such as iron(III) or manganese(II/III) porphyrins, NMR spectroscopy is useless due to their broad resonances, which prevent observation of signal multiplicities. This difficulty has been overcome by using electronic circular dichroism (ECD) spectroscopy as a conformational probe. In a preliminary study, examination of the ECD spectra of H_2BCP*n* ($n = 8, 9$) and of their diamagnetic Ni(II) and Zn(II) complexes has allowed correlations to be drawn between the conformation (observed by NMR) and the sign of the Cotton effect in the Soret region.[5] Bridled chiroporphyrins that are in an αααα conformation (H_2BCP8, **î**) gave a positive ECD signal, while those with a αβαβ conformation (**2̂**, H_2BCP9, [Ni(BCP9)], and [Zn(BCP9)]) gave a negative ECD signal. It has been shown that this empirical correlation could be safely extended to the Mn(III) and Mn(II) complexes in this series, allowing plausible assignments of their solution conformations.[6] For the Mn(III) complexes, the conformation assignment deduced from the composite ECD signal has been corroborated by an X-ray structure determination of [Mn^{III}Cl(BCP10)], which shows a mixture of αααα and αβαβ atropisomers.[2] Accordingly, the square-planar [Mn^{II}(BCP8)] complex, which exhibits a positive ECD signal, has been assigned the C_2-symmetric αααα conformation,[6] similar to that of the Zn(II) complex. These observations suggest that a redox signal can trigger the αααα ↔ αβαβ change of conformations in BCP complexes.

Predicting the stereochemistry of a given BCP complex is a challenging theoretical issue in that the Gibbs free energy G of each of its conformers must be accurately determined for the conformational analysis to be complete. Different factors affecting the free energies of the conformers thus come into play, possibly strengthening or counterbalancing the effects of one another in a subtle manner. We do not intend to consider all of them simultaneously in the present theoretical contribution. Consequently, we will in the following delineate the scope of our study. G divides into a gas-phase contribution G[∅] and an environmental contribution G[env.], for which we shall only consider solvation effects. Given that the solvent-accessible surface area of the open form αβαβ is larger than that of the closed form αααα, solvation is likely to have a large influence on the αααα ↔ αβαβ conformational equilibrium. However, it is not our purpose to investigate here solvation effects. These will be addressed in subsequent studies using a continuum solvation model.[7−10] Besides the calculation of the electronic energy, the determination of G[∅] would necessitate that of the vibration frequencies so as to be able to calculate the entropy, the zero-point energy, and thermal corrections. The BCP complexes are quite large systems for which vibrational analyses are computationally demanding. In the present study, we do not tackle the determination of these frequencies, and therefore, we base our conformational analyses on the determination of the electronic energy differences. *That is, for the time being, we are only concerned with the careful and thorough exploration of the electronic and structural influences of transition metals on the stereochemistry of a chiroporphyrin, namely, BCP8.*

(5) Maheut, G.; Castaings, A.; Pécaut, J.; Lawson Daku, L. M.; Pescitelli, G.; Di Bari, L.; Marchon, J.-C. *J. Am. Chem. Soc.* **2006**, *128*, 6347–6356.

(6) A. Castaings, *Thèse de doctorat de l'université Joseph Fourier*, Grenoble (chapters V−VII). http://tel.archives-ouvertes.fr/tel-00129098 (accessed March 12, 2009).

(7) Cramer, C. J.; Truhlar, D. G. *Chem. Rev.* **1999**, *99*, 2161–2200.

(8) Dong, F.; Wagoner, J. A.; Baker, N. A. *Phys. Chem. Chem. Phys.* **2008**, *10*, 4889–4902.

(9) Chen, J.; Brooks, C. L.III; Khandogin, J. *Curr. Opin. Chem. Biol.* **2008**, *18*, 140–148.

(10) Implicit solvation models allow the calculations of solvation free energies at reasonable computational costs. They also allow one to distinguish between the contributions arising from the electronic and structural relaxations of the considered system upon solvation and those arising from the solute−solvent interactions. Actually, when using an implicit solvation model for studying metalloporphyrins, attention must be paid to the fact that the transition metal cation may exhibit a noticeable affinity for the solvent molecules. In such a case, the chemical identity of the considered system actually changes due to the presence of a more or less pronounced axial coordination by the solvent molecules. These solvent molecules should then be explicitly taken into account, as their presence alters the ligand field around the metal, for instance. For the BCP complexes, this is likely to affect their stereochemistry.

Within this precise framework, we recently applied density functional theory (DFT)[11−14] to the study of the relative stability of the αααα and αβαβ conformers of **1̂** and **2̂**.[5] For either complex, the BCP8 moiety was shown to exhibit in the αααα conformation a dome-shaped porphyrin which slightly contracts and becomes strongly ruffled upon the αααα → αβαβ isomerization, so as to accommodate the alternating up−down meso substituents. For a given conformation of the bridled chiroporphyrin, the metal−nitrogen bonds were found to undergo upon Zn(II) → Ni(II) substitution a shortening of ∼0.1 Å, which is due to the fact that the antibonding level of $d_{x^2-y^2}$ type, which is filled in the d^{10} zinc (II) complex **1̂**, becomes unoccupied in the LS d^8 nickel(II) complex **2̂**. For complex **1̂**, the αααα conformer was found to be the electronically most stable form. By passing to **2̂**, there is a strong stabilization of the αβαβ conformer, consistent with the X-ray structures of αααα-**1̂** and αβαβ-**2̂**. These results indicate that the extent to which the porphyrin macrocycle contracts (respectively, expands) and stabilizes the αβαβ (respectively, αααα) conformation is largely determined by the occupancy of the stereochemically active $d_{x^2-y^2}$ orbital level.[5]

In this paper, we extend our theoretical study of the stereochemistry of BCP8 complexes to two axially coordinated species, namely the d^5 chloroiron(III) [FeCl(BCP8)] (**3̂**) and the d^4 chloromanganese(III) [MnCl(BCP8)] (**4̂**) complexes. DFT is applied to the determination of the most stable conformer of **3̂** in the sextet high-spin (HS) state known to be the electronic ground state of chloroiron(III) porphyrins,[15,16] and also for the complex in the doublet LS state, which is the alternative ground state for iron(III) complexes. By characterizing **3̂** in these two spin states, we aim at probing the influence of the occupation of the antibonding $d_{x^2-y^2}$ orbital level on the relative stability of the atropisomers. This level is indeed singly occupied for **3̂** in the HS state and becomes unoccupied in the LS state. The conformational analysis is performed on **4̂** in the quintet HS state, which is the electronic ground state of chloromanganese(III) porphyrins,[17] and wherein the $d_{x^2-y^2}$ level remains unoccupied. Note that, for [FeCl(BCP8)] and [MnCl (BCP8)] in the αααα conformation, and with regard to the axial ligation by the Cl^- anion, the conformational analysis also accounts for the possibility of the location of the Cl atom within (conformers αααα-$\hat{\mathbf{3}}_{in}$ and αααα-$\hat{\mathbf{4}}_{in}$) or outside (conformers αααα-$\hat{\mathbf{3}}_{out}$ and αααα-$\hat{\mathbf{4}}_{out}$) the cavity provided by the bridles.

In our previous study,[5] the conformational analyses of **1̂** and **2̂** were carried out using the PBE generalized gradient approximation (GGA).[18,19] In the present study, the situation is complicated by the fact that we are also interested in calculating the relative energies of the conformers of **3̂** in the HS and LS states. Indeed, the accurate determination of the electronic energy differences between states of different spin multiplicities is a challenging theoretical task, especially in DFT, in that most density functionals tend to fail. This difficulty met with the DFT methods has been evidenced for iron porphyrin systems (see, for instance, refs 20−22). It is receiving considerable attention, as attested to by the many recent studies aimed at assessing the performances of modern functionals with regard to the energetics of the spin states of transition metal complexes (see, e.g., refs 23−44). For all of the considered complexes, most GGAs—the PBE functional included—overestimate the stability of states of low-spin multiplicity with regard to those of higher multiplicity. The situation does not necessarily improve in passing to the more sophisticated and computationally demanding hybrid and meta-GGA functionals. Thus, hybrid (respectively, meta-GGA) functionals tend to overstabilize states of high (respectively, low) spin multiplicity with respect to those of lower (respectively, higher) multiplicity. Actually, the performance of the hybrid functionals was shown to strongly depend on the amount of the exact exchange which they include,[24,32,36,40−45] and an exact-exchange contribution of about 10% seems to be appropriate for the study of the spin-state energetics in transition metal complexes.[24,32,36,41,42,44] Unfortunately, the good performance shown by a given functional for some complexes does not necessarily extend to other complexes. Still, with the continuous development of new functionals, it can be expected that the situation will improve. In the meantime,

(11) Hohenberg, P.; Kohn, W. *Phys. Rev.* **1964**, *136*, B864–B871.
(12) Kohn, W.; Sham, L. J. *Phys. Rev.* **1965**, *140*, A1133–A1138.
(13) Gunnarsson, O.; Lundqvist, B. I. *Phys. Rev. B* **1976**, *13*, 4274–4298.
(14) Gunnarsson, O.; Lundqvist, B. I. *Phys. Rev. B* **1977**, *15*, 6006.
(15) Scheidt, W. R.; Reed, C. A. *Chem. Rev.* **1981**, *81*, 543–555.
(16) Mazzanti, M.; Marchon, J.-C.; Wojaczyński, J.; Wołowiec, S.; Latos-Grażyński, L.; Shang, M.; Scheidt, W. R. *Inorg. Chem.* **1998**, *37*, 2476–2481.
(17) Scheidt, W. R. In *The Porphyrin Handbook*; Kadish, K. M., Smith, K. M., Guilard, R., Eds.; Academic Press: San Diego, 2000; Vol. *3*.
(18) Perdew, J. P.; Burke, K.; Ernzerhof, M. *Phys. Rev. Lett.* **1996**, *77*, 3865–3868.
(19) Perdew, J. P.; Burke, K.; Ernzerhof, M. *Phys. Rev. Lett.* **1997**, *78*, 1396.
(20) Smith, D. M. A.; Dupuis, M.; Straatsma, T. P. *Mol. Phys.* **2005**, *103*, 273–278.
(21) Liao, M.-S.; Watts, J. D.; Huang, M.-J. *J. Phys. Chem. A* **2007**, *111*, 5927–5935.
(22) Ghosh, A.; Taylor, P. R. *Curr. Opin. Chem. Biol.* **2003**, *7*, 113–124.
(23) Paulsen, H.; Duelund, L.; Winkler, H.; Toftlund, H.; Trautwein, A. X. *Inorg. Chem.* **2001**, *40*, 2201–2204.
(24) Reiher, M.; Salomon, O.; Hess, B. A. *Theor. Chem. Acc.* **2001**, *107*, 48–55.
(25) Salomon, O.; Reiher, M.; Hess, B. A. *J. Chem. Phys.* **2002**, *117*, 4729–4737.
(26) Poli, R.; Harvey, J. N. *Chem. Soc. Rev.* **2003**, *32*, 1–8.
(27) Swart, M.; Groenhof, A. R.; Ehlers, A. W.; Lammertsma, K. *J. Phys. Chem. A* **2004**, *108*, 5479–5483.
(28) Paulsen, H.; Trautwein, A. X. *Top. Curr. Chem.* **2004**, *235*, 197–219.
(29) Deeth, R. J.; Fey, N. *J. Comput. Chem.* **2004**, *25*, 1840–1848.
(30) Fouqueau, A.; Mer, S.; Casida, M. E.; Lawson Daku, L. M.; Hauser, A.; Mineva, T. *J. Chem. Phys.* **2004**, *120*, 9473–9486.
(31) Fouqueau, A.; Casida, M. E.; Lawson Daku, L. M.; Hauser, A.; Neese, F. *J. Chem. Phys.* **2005**, *122*, 044110.
(32) Lawson Daku, L. M.; Vargas, A.; Hauser, A.; Fouqueau, A.; Casida, M. E. *ChemPhysChem* **2005**, *6*, 1393–1410.
(33) Ganzenmüller, G.; Berkaïne, N.; Fouqueau, A.; Casida, M. E.; Reiher, M. *J. Chem. Phys.* **2005**, *122*, 234321.
(34) Vargas, A.; Zerara, M.; Krausz, E.; Hauser, A.; Lawson Daku, L. M. *J. Chem. Theory Comput.* **2006**, *2*, 1342–1359.
(35) Pierloot, K.; Vancoillie, S. *J. Chem. Phys.* **2006**, *125*, 124303.
(36) Zein, S.; Borshch, S. A.; Fleurat-Lessard, P.; Casida, M. E. Chermette, H. *J. Chem. Phys.* **2007**, *126*, 014105.
(37) Krivokapic, I.; Zerara, M.; Lawson Daku, M.; Vargas, A. Enachescu, C.; Ambrus, C.; Tregenna-Piggott, P.; Amstutz, N.; Krausz, E.; Hauser, A. *Coord. Chem. Rev.* **2007**, *251*, 364–378.
(38) Scherlis, D. A.; Cococcioni, M.; Sit, P.; Marzari, N. *J. Phys. Chem. B* **2007**, *111*, 7384–7391.
(39) Pierloot, K.; Vancoillie, S. *J. Chem. Phys.* **2008**, *128*, 034104.
(40) Jensen, K. P.; Roos, B. O.; Ryde, U. *J. Chem. Phys.* **2007**, *126*, 014103.
(41) Reiher, M. *Inorg. Chem.* **2002**, *41*, 6928–6935.
(42) Schenk, G.; Pau, M. Y. M.; Solomon, E. I. *J. Am. Chem. Soc.* **2004**, *126*, 505–515.
(43) Furche, F.; Perdew, J. P. *J. Chem. Phys.* **2006**, *124*, 044103.
(44) Jensen, K. P. *Inorg. Chem.* **2008**, *47*, 10357–10365.
(45) Neese, F. *J. Biol. Inorg. Chem.* **2006**, *11*, 702–711.

great care must be taken in the application of DFT to the determination of the relative energies of different spin states.

In this study, we have chosen to employ the RPBE GGA,[46] which gave good results for the spin-state energetics of iron complexes.[29−32] For comparison purposes, we also studied **1̂** and **2̂** with the RPBE functional. We furthermore assessed the performance of this functional by investigating the stereochemistry of two experimentally well-characterized complexes of tetramethylchiroporphyrin (TMCP), namely, the chloroiron(III) complex [FeCl(TMCP)] (**3̈**)[16] and the chloromanganese(III) complex [MnCl(TMCP)] (**4̈**),[47] which are similar to **3̂** and **4̂** but are devoid of straps. Both are HS species and have been isolated as $\alpha\beta\alpha\beta$ conformers. A comparison of the results obtained for the chloroiron(III) and chloromanganese(III) complexes of TMCP with those obtained for their BCP8 counterparts will help us discuss the influence of the short bridles in detail.

2. Computational Details

Calculations were carried out with the Amsterdam Density Functional (ADF) program package,[48,49] using basis sets from the ADF basis set database. ADF uses Slater-type orbital (STO) functions, and the set of STO functions used corresponds the S' set of ref 5. It consists of a triple-ζ polarized basis set TZP for the Mn, Fe, Ni, and Zn atoms; a double-ζ polarized basis set DZP for the N, Cl, C, and O atoms; and a double-ζ basis set DZ for the H atoms. The core shells were frozen up to the 3p level for Mn, Fe, Ni, and Zn,; up to the 2p level for Cl; and up to the 1s level for C, O, and N. The general accuracy parameter "accint" was set to 4.5, which is quite a high value, and the other program parameters were kept to their default values. Calculations were run restricted for the zinc(II) and LS nickel(II) complexes. They were run unrestricted for the chloromanganese(III) complexes with M_S, the projection of the total electronic spin along a reference axis, constrained to $M_S = +2$. For the chloroiron(III) complexes, they were also run unrestricted, with M_S constrained to $M_S = +1/2$ and $M_S = +5/2$ for characterizing the complexes in the LS and HS states, respectively.

In all cases, the symmetry of the complexes was constrained to C_2. Note that the C_2 symmetry operation interchanges the pyrrole rings (1) and (1′) and the (2) and (2′) rings (see Figure 1), and that one therefore verifies for the metal−nitrogen distances: $M-N_i = M-N_{i'}$, with M = Zn, Ni, Fe, and Mn and $i = 1$ and 2. The important structural parameters for characterizing the geometries of the BCP8 and TMCP complexes in the $\alpha\alpha\alpha\alpha$ and $\alpha\beta\alpha\beta$ conformations are (*i*) the M−Cl bond length (in chloroiron(III) and chloromanganese(III) complexes); (*ii*) the average metal−nitrogen bond length, which gives a measure of the contraction of the porphinato core;[15] (*iii*) the displacement of the metal atom out of the mean plane of the 24 atoms of the porphyrin core M−Ct (Ct: the projection of the metal atom on the mean plane); (*iv*) the root-mean-square (rms) out-of-plane displacement Δ_{rms}, which provides a measure of the deviation of the porphyrin macrocycle from planarity and which is given by[50]

$$\Delta_{RMS} = \sqrt{\frac{1}{24}\sum_{k=1}^{24}\delta_k^2} \qquad (1)$$

where δ_k is the orthogonal displacement of the kth atom of the macrocycle from the mean plane; and (*v*) the average torsional angle $C_\alpha-N-N-C_\alpha$ between opposite pyrrole rings, which gives a measure of the ruffling of the porphyrin macrocycle and which is also known as the ruffling angle.[50,51]

In order to further characterize the out-of-plane distortion of the porphyrin macrocycle in the investigated complexes, their structures have been analyzed using the normal-coordinate structural decomposition (NSD) scheme of Shelnutt et al.[52−54] In this scheme, the out-of-plane distortion of a given macrocycle is described by displacements along the lowest-frequency out-of-plane normal coordinates of the "ideal" D_{4h}-symmetric macrocycle. This thus gives the amounts of the saddling (*sad*, b_{2u}), ruffling (*ruf*, b_{1u}), doming (*dom*, a_{2u}), waving ([*wav* (*x*), *wav* (*y*)], e_g), and propellering (*pro*, a_{1u}) deformation types involved in the out-of-plane distortion of the considered macrocycle. Note that, within C_2, the waving deformation types do not contribute to out-of-plane distortion.

3. Results and Discussion

3.1. The Zinc(II) and Low-Spin Nickel(II) Complexes. In order to be consistent within the series of investigated BCP8 complexes, the conformational analysis of **1̂** and **2̂** has been reconducted at the RPBE/S' level. In this section, we compare the new results with those previously obtained with the PBE functional using the same basis set S'. The results thus obtained with the two functionals for the geometries of the $\alpha\alpha\alpha\alpha$ and $\alpha\beta\alpha\beta$ conformers of the two complexes are summarized in Table 1.

Inspection of Table 1 indicates that the geometries obtained with the two functionals tend to be very close. Indeed, when one considers for a given conformer of **1̂** or **2̂** the RPBE and PBE parameter values, one notes that these values typically differ by less than ∼0.03 Å for the M−N bond lengths (M = Zn, Ni), the out-of-plane metal atom displacement M−Ct, and the rms out-of-plane displacement Δ_{rms}, and by less than ∼2° for the ruffling angle $C_\alpha-N-N-C_\alpha$. Still, for the $\alpha\beta\alpha\beta$ atropisomer of **1̂** and for the $\alpha\beta\alpha\beta$ atropisomer of **2̂** to a lesser extent, noticeably larger differences exist between the RPBE and PBE values of the Δ_{rms} and $C_\alpha-N-N-C_\alpha$ parameters. Figure 3 summarizes the NSD results for the calculated and the available X-ray structures of the conformers of **1̂** and **2̂**. For $\alpha\beta\alpha\beta$-**1̂**, the analysis of these data shows that

(46) Hammer, B.; Hansen, L. B.; Nørskov, J. K. *Phys. Rev. B* **1999**, *59*, 7413–7421.
(47) Simonato, J.-P.; Pécaut, J.; Scheidt, W. R.; Marchon, J.-C. *Chem. Commun.* **1999**, 989–990.
(48) *Amsterdam Density Functional Program*; Theoretical Chemistry, Vrije Universiteit: Amsterdam, The Netherlands. http://www.scm.com (accessed Nov. 2, 2008).
(49) te Velde, G.; Bickelhaupt, F. M.; Baerends, E. J.; Fonseca Guerra, C.; van Gisbergen, S. J. A.; Snijders, J. G.; Ziegler, T. *J. Comput. Chem.* **2001**, *22*, 931–967.
(50) Jentzen, W.; Turowska-Tyrk, I.; Scheidt, W. R.; Shelnutt, J. A. *Inorg. Chem.* **1996**, *35*, 3559–3567.
(51) Song, Y.; Haddad, R. E.; Jia, S.-L.; Hok, S.; Olmstead, M. M.; Nurco, D. J.; Schore, N. E.; Zhang, J.; Ma, J.-G.; Smith, K. M.; Gazeau, S.; Pécaut, J.; Marchon, J.-C.; Medforth, C. J.; Shelnutt, J. A. *J. Am. Chem. Soc.* **2005**, *127*, 1179–1192.
(52) Jentzen, W.; Song, X.-Z.; Shelnutt, J. A. *J. Phys. Chem. B* **1997**, *101*, 1684–1699.
(53) Shelnutt, J. A.; Song, X.-Z.; Ma, J.-G.; Jia, S.-L.; Jentzen, W.; Medforth, C. J. *Chem. Soc. Rev.* **1998**, *27*, 31–41.
(54) Jentzen, W.; Ma, J.-G.; Shelnutt, J. A. *Biophys. J.* **1998**, *74*, 753–763.

Table 1. Metal−Ligand Bond Lengths, Out-of-Plane Displacement (M−Ct) of the Metal Atom from the 24-Atom Mean Plane (Å), Root-Mean-Square Out-of-Plane Displacement (Δ_{RMS}, in Å), and Ruffling Angle ($C_\alpha-N-N-C_\alpha$) in the Optimized Geometries of the Conformers of the BCP8 Complexes $\hat{\mathbf{1}}$ and $\hat{\mathbf{2}}$[a]

			M−N_1	M−N_2	M−N[b]	M−Ct	Δ_{rms}	$C_\alpha-N-N-C_\alpha$
			Optimized Geometries					
αααα-$\hat{\mathbf{1}}$		RPBE	2.101	2.076	2.089	0.222	0.152	3.4
		PBE	2.081	2.067	2.074	0.238	0.153	3.2
αβαβ-$\hat{\mathbf{1}}$		RPBE	2.034	2.071	2.054	0.000	0.333	26.3
		PBE	2.052	2.062	2.057	0.003	0.188	18.7
αααα-$\hat{\mathbf{2}}$		RPBE	2.012	1.985	1.999	0.163	0.116	4.1
		PBE	1.994	1.972	1.983	0.175	0.126	5.7
αβαβ-$\hat{\mathbf{2}}$		RPBE	1.933	1.958	1.946	0.000	0.427	35.5
		PBE	1.934	1.945	1.940	0.022	0.353	36.3
			X-Ray Structures					
αααα-$\hat{\mathbf{1}}$[c]	(Zn_1)		2.046, 2.027	2.045, 2.046	2.041	0.147	0.128	3.1
	(Zn_2)		2.034, 2.031	2.029, 2.025	2.030	0.111	0.117	4.3
αβαβ-$\hat{\mathbf{2}}$[c]	(Ni_1)		1.921, 1.925	1.901, 1.915	1.916	0.006	0.373	38.1
	(Ni_2)		1.921, 1.921	1.909, 1.917	1.917	0.014	0.386	37.6

[a] Results of calculations at the RPBE/S' level (this work) and at the PBE/S' level (taken from ref 5). The values found for these parameters in the X-ray structure of the complex are also given. [b] Average metal−nitrogen distance. [c] The crystal of [Zn(BCP8)] ($\hat{\mathbf{1}}$) or [Ni(BCP8)] ($\hat{\mathbf{2}}$) contains two independent molecules: (Zn_1, Zn_2) or (Ni_1, Ni_2), which have no symmetry. The distinct M−N_i and M−$N_{i'}$ distances (i = 1, 2) found for each molecule are reported (from ref 1).

the out-of-plane distortion predicted at the PBE level for the porphyrin core consists almost exclusively of a large *ruf* deformation of 0.9 Å, the contributions from the other deformations being comparatively vanishing. In passing to the RPBE structure of αβαβ-$\hat{\mathbf{1}}$, there is a 0.4 Å increase of the *ruf* deformation, which goes with the large increase of 7.6° observed for the ruffling angle $C_\alpha-N-N-C_\alpha$ (Table 1). But there is also a second and large negative displacement (− 1.0 Å) along the *sad* deformation, which, along with the larger *ruf* deformation, explains the large difference observed between the PBE and RPBE values of Δ_{rms}.

For αβαβ-$\hat{\mathbf{2}}$, the use of the two functionals leads to structures which exhibit similar *ruf* deformations of ≈1.7 Å. This agrees with the fact that similar values are obtained for $C_\alpha-N-N-C_\alpha$ at both levels (Table 1). The PBE and RPBE structures present also *sad* deformations of −0.3 Å and −1.2 Å, respectively. The large difference between the PBE and RPBE values of the displacement along this last deformation coordinate explains the large difference observed between the PBE and RPBE values of Δ_{rms} (Table 1). Actually, for the calculated structures of either conformer of $\hat{\mathbf{1}}$ or $\hat{\mathbf{2}}$, the displacement along the *sad* deformation is predicted to be more negative (or less positive) in the RPBE structure than in PBE structure, this trend being more pronounced for the αβαβ conformers (Figure 3). Besides these differences, there is an overall good agreement between the theoretical values of the key structural parameters of Table 1 and Figure 3. This shows that the optimized geometries of a given conformer of the Zn(II) or LS Ni(II) complex are all quite similar to one another, irrespective of the theoretical level. In addition, for αααα-$\hat{\mathbf{1}}$ and αβαβ-$\hat{\mathbf{2}}$, the inspection of Table 1 and Figure 3 shows that the calculated calculated geometries compare quite well with the experimental ones. Finally, it is worth noting that, although the porphyrin core is predominantly domed in the αααα conformation, it also exhibits noticeable ruffling and saddling (Figure 3).

Table 2 gives the calculated PBE and RPBE values of the energy difference between the two conformers, $\Delta E_{cnf} = E_{min}(\alpha\beta\alpha\beta) - E_{min}(\alpha\alpha\alpha\alpha)$. The two functionals give for $\hat{\mathbf{2}}$ small ΔE_{cnf} values in agreement with each other, which corresponds to a best estimate of about 800−900 cm^{-1} for the isolated complex. For complex $\hat{\mathbf{1}}$, both functionals predict large but quite distinct energy differences: ΔE_{cnf} = 2769 cm^{-1} at the PBE level and ΔE_{cnf} = 4106 cm^{-1} at the RPBE level. Given that there are no data with which these values could be compared, it is difficult to tell a priori which functional performs best. However, the superior performance shown by the RPBE functional for the energetics of various phenomena involving transition metal compounds (chemisorption energetics of atoms and molecules on transition metal surfaces,[46] first CO dissociation energies of transition metal carbonyls,[55] and spin-state energetics of iron complexes[29−32]) suggests that the PBE functional actually underestimates the gas-phase value of ΔE_{cnf} for $\hat{\mathbf{1}}$ and, consequently, that our best estimate of ΔE_{cnf} for the Zn(II) complex corresponds to the RPBE value of 4106 cm^{-1}.

3.2. The Chloroiron(III) and Chloromanganese(III) TMCP Complexes. In this section, we further assess the reliability of the DFT method used by applying it first to the study of the stereochemistry of the two TMCP complexes. The calculations targeted at the conformational analysis of the chloroiron(III) and chloromanganese(III) TMCP complexes led to the characterization of the αααα-$\ddot{\mathbf{3}}_{in}$, αααα-$\ddot{\mathbf{3}}_{out}$, and αβαβ-$\ddot{\mathbf{3}}$ conformers of the former complex in the LS ^{2}B and the HS ^{6}A states and to that of the αααα-$\ddot{\mathbf{4}}_{in}$, αααα-$\ddot{\mathbf{4}}_{out}$, and αβαβ-$\ddot{\mathbf{4}}$ conformers of the latter complex in the HS ^{5}A state (see Supporting Information (SI)).

3.2.1. Structures. The optimized LS and HS structures of a given conformer of $\ddot{\mathbf{3}}$ are very alike and also resemble the structure obtained for this same conformer in the case of the HS $\ddot{\mathbf{4}}$ complex. These structures are illustrated in Figure 4, which shows the optimized HS geometries of αβαβ-$\ddot{\mathbf{3}}$, αααα-$\ddot{\mathbf{3}}_{in}$, and αααα-$\ddot{\mathbf{3}}_{out}$. As can

(55) Matveev, A.; Staufer, M.; Mayer, M.; Rösch, N. *Int. J. Quantum Chem.* **1999**, *75*, 863–873.

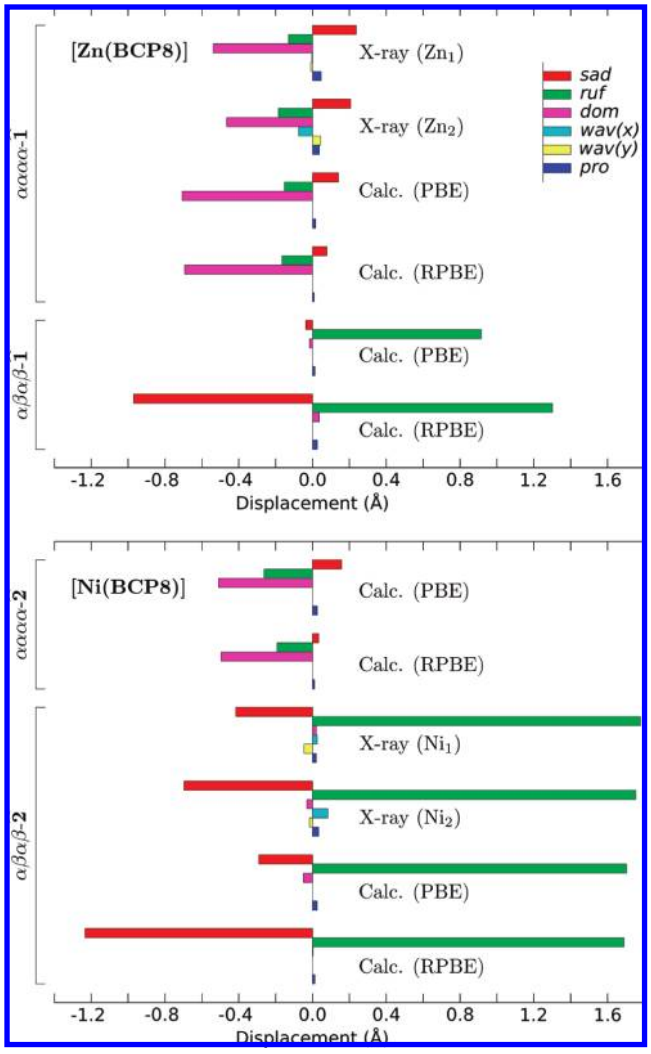

Figure 3. NSD results for the calculated geometries of the αααα and αβαβ conformers of **1̂** and **2̂**. The NSD results obtained for the X-ray structures of αααα-**1̂** and αβαβ-**2̂** are also reported (the crystal of αααα-**1̂** or αβαβ-**2̂** contains two independent molecules: (Zn_1, Zn_2) or (Ni_1, Ni_2); from ref 1).

Table 2. Calculated Values (cm^{-1}) of the Electronic Difference $\Delta E_{cnf} = E_{min}(\alpha\beta\alpha\beta) - E_{min}(\alpha\alpha\alpha\alpha)$ in the BCP8 Complexes **1̂** and **2̂**[a]

theoretical level	**1̂**	**2̂**
PBE	+2769	+843
RPBE	+4106	+872

[a] Results of calculations at the RPBE/*S*′ level (this work) and at the PBE/*S*′ level (taken from ref 5).

be inferred from Figure 4, the optimized geometries of the αβαβ conformers of **3̈** and **4̈** exhibit a ruffling of the porphyrin macrocycle and inwardly directed carbonyl groups. These two features are also present in the X-ray structures of αβαβ-**3̈**[16] and αβαβ-**4̈**.[47] As for the two αααα conformers of the TMCP complexes, their predicted structures exhibit a doming of the porphyrin core and ester moieties which have their carbonyl group outwardly directed.

Table 3 gives the values of the key structural parameters that help characterize the optimized geometries of the αααα and αβαβ conformers of **3̈** and **4̈**. The values found for these parameters in the experimental geometries of

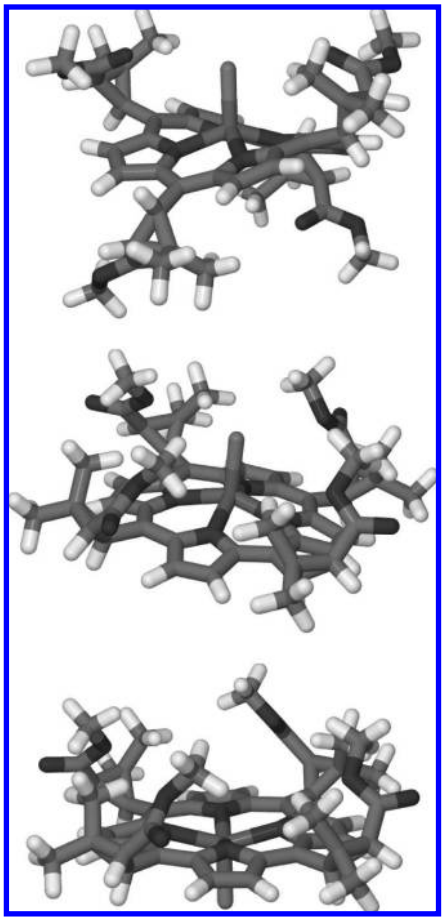

Figure 4. Optimized HS geometries of αβαβ-**3̈** (top), αααα-$\ddot{\mathbf{3}}_{in}$ (middle), and αβαβ-$\ddot{\mathbf{3}}_{out}$ (bottom).

their αβαβ conformers are also given. There is good agreement between them and their theoretical counterparts. Actually, the porphyrin macrocycle is predicted to be sligthly more expanded and less ruffled than experimentally observed. Indeed, the optimized metal−nitrogen bonds (respectively, the calculated values of $C_\alpha-N-N-C_\alpha$) are about 3% longer (respectively, 10% smaller) than the experimental ones. Such a discrepancy is very likely due to the neglect of the crystal packing forces in our calculations performed for the complexes in the gas phase.

Upon the αααα-$\ddot{\mathbf{3}}_{in}$ → αααα-$\ddot{\mathbf{3}}_{out}$ change of conformations for **3̈** in the LS or HS state, or similarly upon the αααα-$\ddot{\mathbf{4}}_{in}$ → αααα-$\ddot{\mathbf{4}}_{out}$ change of conformations for HS **4̈**, the largest change is observed for the metal atom out-of-plane displacement M−Ct, which decreases in all cases by ≈0.4 Å (Table 3). The strong influence of the location of the chloride above or below the porphyrin macrocycle on the M−Ct parameter follows from the fact that the bonding interaction between the transition metal and Cl atoms shifts the metal atom toward the Cl atom. For the two TMCP complexes, one also observes upon the αααα → αβαβ atropisomerisation a large increase of Δ_{rms} and of $C_\alpha-N-N-C_\alpha$, which is indicative of the strong ruffling of the porphyrin core. As expected upon ruffling,[15] there is a concomitant contraction of the porphyrin core, which translates into a decrease of the metal−nitrogen distances by about 0.05 Å. Figure 5 summarizes the NSD results

Table 3. Metal−Ligand Bond Lengths, Out-of-Plane Displacement (M−Ct) of the Metal Atom from the 24-Atom Mean Plane (Å), Root-Mean-Square Out-of-Plane Displacement (Δ_{RMS}, in Å), and Ruffling Angle ($C_\alpha-N-N-C_\alpha$) in the Optimized Geometries of the Conformers of the Complexes [FeCl(TMCP)] (**3̈**) and [MnCl(TMCP)] (**4̈**)[a]

	spin state	M−N$_1$[b]	M−N$_2$[b]	M−N[c]	M−Cl	M−Ct	Δ_{rms}	$C_\alpha-N-N-C_\alpha$
				Optimized Geometries				
αααα-**3̈**$_{in}$	HS	2.146	2.149	2.148	2.268	0.830	0.157	3.3
	LS	2.023	2.024	2.024	2.225	0.395	0.124	2.7
αααα-**3̈**$_{out}$	HS	2.126	2.133	2.130	2.248	0.442	0.115	3.7
	LS	2.019	2.020	2.020	2.211	0.017	0.123	3.7
αβαβ-**3̈**	HS	2.102	2.109	2.106	2.242	0.710	0.366	35.8
	LS	1.976	1.976	1.976	2.205	0.215	0.374	37.3
αααα-**4̈**$_{in}$	HS	2.077	2.078	2.078	2.363	0.572	0.145	3.3
αααα-**4̈**$_{out}$	HS	2.061	2.067	2.064	2.341	0.165	0.115	3.6
αβαβ-**4̈**	HS	2.025	2.032	2.029	2.339	0.413	0.377	37.3
				X-Ray Structures				
αβαβ-**3̈**[d]	HS	2.027	2.040	2.034	2.207	0.640	0.395	40.3
αβαβ-**4**[d]	HS	1.968	1.981	1.975	2.347	0.437	0.420	43.1

[a] Values found for these parameters in the X-ray structures of αβαβ-**3̈** and αβαβ-**4̈** are given for comparison purposes. [b] The labeling of the nitrogen atoms is arbitrary. [c] Average metal−nitrogen distance. [d] The experimental structures of αβαβ-**3̈**[16] and αβαβ-**4̈**[47] are of C_2 symmetry.

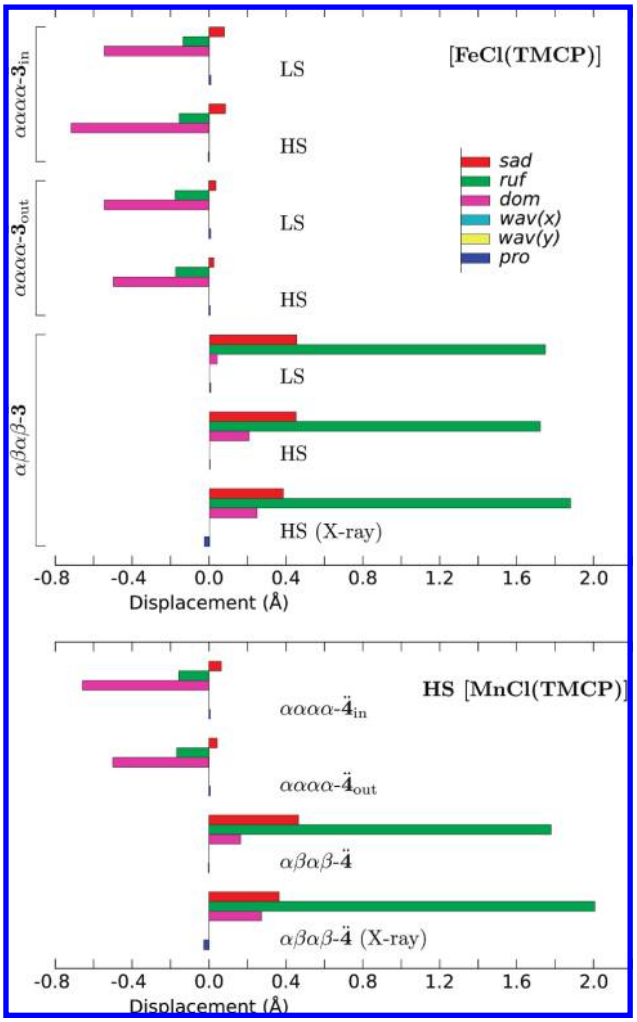

Figure 5. NSD results for the calculated geometries of the conformers of **3̈** and **4̈**. The NSD results obtained for the X-ray structures of αβαβ-**3̈**[16] and αβαβ-**4̈**[47] are also reported.

for the calculated and available X-ray structures of **3̈** and **4̈**.

There is a very satisfactory agreement between the NSD data obtained for the calculated and X-ray structures of HS αβαβ-**3̈** or HS αβαβ-**4̈**. For **3̈** and **4̈** in their different spin-states, the out-of-plane distortion of the macrocycle proves to be remarkably conserved among the αααα conformers and among the αβαβ conformers (Figure 5). The conservation of the conformation of the macrocycle among the αααα or αβαβ conformers of both species is also reflected by the similar values found for Δ_{rms} and for $C_\alpha-N-N-C_\alpha$ (Table 3). These conserved characteristic distortions can be considered as optimal in that they probably help maximize the bonding interactions between the M−Cl (M = Fe, Mn) and TCMP moieties of the complexes in the αααα or αβαβ forms. In the αααα conformation, the porphyrin core is predominantly domed with noticeable *ruf* and *sad* deformations. Furthermore, the amounts of the displacements along these deformation coordinates are rather weakly influenced by the α or β location of the chloride ligand. In passing to the αβαβ conformation, the core becomes predominantly ruffled with significant *sad* and *dom* deformations.

For the three conformers of **3̈**, the Fe−N and Fe−Cl bonds lengthen by about 0.12 Å and 0.04 Å, respectively, when passing from the LS to the HS state. This is due to the population of the antibonding $d_{x^2-y^2}$ and d_{z^2} metallic levels. The optimized Fe−N bond lengths are slightly larger than the nominal equatorial Fe−N bond lengths of 1.990 and 2.069 Å reported for iron(III) porphyrins in the LS and HS spin states, respectively.[15] In fact, there is no reason as to why they should strictly match. Nevertheless, the HS−LS Fe−N bond length difference of ∼0.12 Å is in relatively good agreement with the ∼0.08 Å difference between the nominal HS and LS Fe−N bond lengths, and also with the average Fe−N bond length variation of about 0.15 Å observed in iron(III) spin-crossover complexes with ligating N atoms.[56,57] The LS → HS change of spin states is accompanied for all conformers of **3̈** by a strong increase of the Fe−Ct distance of ca. 0.4−0.5 Å. This large enhancement of the iron out-of-plane displacement may be the result of the combined effects of the weakening

(56) Milne, A. M.; Maslen, E. N. *Acta Crystallogr.* **1988**, *B44*, 254–259.
(57) Oshio, H.; Toriumi, K.; Maeda, Y.; Takashima, Y. *Inorg. Chem.* **1991**, *30*, 4252–4260.

of the Fe−N bonds and of the repulsion between the axial ligand and the porphyrin macrocycle, as has been evidenced for axially ligated iron(II) porphyrins.[58]

3.2.2. Energetics. We first consider the results obtained for the spin-state energetics of $\ddot{\mathbf{3}}$. Table 4 gives the values of the LS−HS electronic energy difference, $\Delta E_{LH} = E_{min}^{LS} - E_{min}^{HS}$, found for its three conformers.

These values are all positive. That is, the HS state is predicted to be the most stable spin state for the three conformers of $\ddot{\mathbf{3}}$. This result is in agreement with the fact that, as effectively observed for $\ddot{\mathbf{3}}$,[16] the chloroiron(III) porphyrins are experimentally found to be HS species.[15,16] The ΔE_{LH} values found for the αααα-$\ddot{\mathbf{3}}_{in}$ and αααα-$\ddot{\mathbf{3}}_{out}$ conformers are large (+2044 and +1408 cm^{-1}, respectively), and they are far greater than the value of +351 cm^{-1} obtained for the αβαβ-$\ddot{\mathbf{3}}$ atropisomer. This noticeable stabilization of the LS state with regard to the HS state upon the αααα → αβαβ atropisomeriszation will be discussed below.

Table 5 gives the electronic energies of the different conformers of $\ddot{\mathbf{3}}$ in the LS and HS states as well as those of the conformers of HS $\ddot{\mathbf{4}}$. For both complexes, the energies are given relative to the energy of their respective electronically most stable forms, namely, the HS αααα-$\ddot{\mathbf{3}}_{in}$ and αααα-$\ddot{\mathbf{4}}_{in}$ conformers. Actually, the two HS complexes are experimentally isolated as αβαβ conformers. Inspection of Table 5 shows that the HS αβαβ atroposisomers of $\ddot{\mathbf{3}}$ and $\ddot{\mathbf{4}}$ are predicted to be close in energy to the HS αααα-$\ddot{\mathbf{3}}_{in}$ and αααα-$\ddot{\mathbf{4}}_{in}$ conformers, lying above them by only +372 and +282 cm^{-1}, respectively. This situation is similar to that found for the LS nickel(II) BCP8 complex $\hat{\mathbf{2}}$. Indeed, although $\hat{\mathbf{2}}$ is experimentally isolated as the αβαβ conformer, its electronically most stable form is predicted to be the αααα conformer, with a small energy difference of +872 cm^{-1} (RPBE results of Table 2). Such discrepancies can be ascribed to the noninclusion in the analysis of the influences of factors other than those that are electronic, namely, environmental effects, zero-point energy, and entropy contributions to the free energies of the isolated conformers. These factors must indeed be taken into account in order to have the whole picture regarding the stereochemistry of the studied chiroporphyrins. Still, as emphasized in the Introduction, we remain focused for the time being on the study of the electronic and structural influences of the metals.

For $\ddot{\mathbf{3}}$ in the HS state, the electronically most stable conformer is αααα-$\ddot{\mathbf{3}}_{in}$, with αβαβ-$\ddot{\mathbf{3}}$ and αααα-$\ddot{\mathbf{3}}_{out}$ respectively +372 and +2017 cm^{-1} higher in energy:

$$HS\alpha\alpha\alpha\alpha\text{-}\ddot{\mathbf{3}}_{in} < HS\alpha\beta\alpha\beta\text{-}\ddot{\mathbf{3}} < HS\alpha\alpha\alpha\alpha\text{-}\ddot{\mathbf{3}}_{out} \quad (2)$$

and the electronically most stable conformer is αβαβ-$\ddot{\mathbf{3}}$ in the LS state, with αααα-$\ddot{\mathbf{3}}_{in}$ and αααα-$\ddot{\mathbf{3}}_{out}$ respectively +1321 and +2702 cm^{-1} higher in energy:

$$LS\alpha\beta\alpha\beta\text{-}\ddot{\mathbf{3}} < LS\alpha\alpha\alpha\alpha\text{-}\ddot{\mathbf{3}}_{in} < LS\alpha\alpha\alpha\alpha\text{-}\ddot{\mathbf{3}}_{out} \quad (3)$$

The large stabilization of the αβαβ conformation with regard to the αααα conformations upon the HS → LS change of spin states is due to the fact that the LS Fe−N bonds are ≈0.1 Å shorter than the HS Fe−N bonds, and that the contraction of the porphyrin macrocycle stabilizes the αβαβ conformation with regard to the αααα conformation. Such a stabilization of the αβαβ conformation with regard to the αααα conformation is observed for BCP8 complexes upon the Zn(II) → Ni(II) substitution, which, similarly, gives rise to a shortening of the metal−nitrogen bonds of ∼0.1 Å (Tables 1 and 2). As in the case of the BCP8 complexes $\hat{\mathbf{1}}$ and $\hat{\mathbf{2}}$, the results obtained for the chloroiron(III) TMCP complex show that the control of the expansion of the porphyrin core achieved by varying the occupancy of the $d_{x^2-y^2}$ antibonding level provides an effective means of tuning the stereochemistry of complexes of such chiroporphyrins.

For $\ddot{\mathbf{3}}$ in the LS or HS state and for HS $\ddot{\mathbf{4}}$, the electronically most stable αααα conformers are predicted to be αααα-$\ddot{\mathbf{3}}_{in}$ and αααα-$\ddot{\mathbf{4}}_{in}$. As put forth by Mazzanti et al.[59] in discussing the preferences of axial ligands for αααα or αβαβ conformers of Zn(II) complexes of substituted chiroporphyrins, the preferential location of the chloride anion on the α side of the macrocycle involves the combined effect of (*i*) a minimization of the steric repulsion between the substituents and the anion and (*ii*) a maximization of their attractive van der Waals interactions. One must also consider (*iii*) the repulsion between the chloride anion and the negatively charged macrocycle,[58,60] which is governed by the distance of the chloride to the macrocycle mean plane: Cl−Ct = M−Ct + M−Cl. Thus, for the αααα conformers of $\ddot{\mathbf{3}}$ in either spin state and for those of HS $\ddot{\mathbf{4}}$, the large energy increase observed in moving Cl^- from the α to the β location is correlated with the increase of repulsion which goes with the decrease of the Cl−Ct distance of as much as ≈0.4 Å.

The ordering of the energies of the three conformers of $\ddot{\mathbf{3}}$ in the HS state (eq 2) turns out to be the reverse ordering of their Cl−Ct distances: 3.098, 2.952, and 2.690 Å for

Table 4. Calculated Values of the LS−HS Electronic Energy Difference ΔE_{LH} (cm^{-1}) for the Three Conformers of the Chloroiron(III) TMCP Complex $\ddot{\mathbf{3}}$

αααα-$\ddot{\mathbf{3}}_{in}$	αααα-$\ddot{\mathbf{3}}_{out}$	αβαβ-$\ddot{\mathbf{3}}$
+2044	+1408	+351

Table 5. Calculated Electronic Energies of the Three Conformers of $\ddot{\mathbf{3}}$ in the LS and HS States and of the Three Conformers of the HS $\ddot{\mathbf{4}}$ Species[a]

αααα-$\ddot{\mathbf{3}}_{in}$		αααα-$\ddot{\mathbf{3}}_{out}$		αβαβ-$\ddot{\mathbf{3}}$	
HS	LS	HS	LS	HS	LS
0	+2044	+2017	+3425	+372	+723
HS αααα-$\ddot{\mathbf{4}}_{in}$		HS αααα-$\ddot{\mathbf{4}}_{out}$		HS αβαβ-$\ddot{\mathbf{4}}$	
0		+2522		+282	

[a] For both complexes, the energy of the most stable form is taken as the zero of the energy scale.

(58) Ugalde, J.; Dunietz, B.; Dreuw, A.; Head-Gordon, M.; Boyd, R. J. *J. Phys. Chem. A* **2004**, *108*, 4653–4657.

(59) Mazzanti, M.; Marchon, J.-C.; Shang, M.; Scheidt, W. R.; Jia, S.; Shelnutt, J. A. *J. Am. Chem. Soc.* **1997**, *119*, 12400–12401.

(60) Chanda, A.; Popescu, D.-L.; de Oliveira, F. T.; Bominaar, E. L.; Ryabov, A. D.; Münck, E.; Collins, T. J. *J. Inorg. Biochem.* **2006**, *100*, 606–619.

αααα-$\ddot{\mathbf{3}}_{in}$, αβαβ-$\ddot{\mathbf{3}}$, and αααα-$\ddot{\mathbf{3}}_{out}$, respectively. This is also the case for HS $\ddot{\mathbf{4}}$ since the ordering of the energies of its conformers is

$$HS\alpha\alpha\alpha\alpha\text{-}\ddot{\mathbf{4}}_{in} < HS\alpha\beta\alpha\beta\text{-}\ddot{\mathbf{4}} < HS\alpha\alpha\alpha\alpha\text{-}\ddot{\mathbf{4}}_{out} \quad (4)$$

and the Cl−Ct distances are 2.935, 2.752, and 2.506 Å for αααα-$\ddot{\mathbf{4}}_{in}$, αβαβ-$\ddot{\mathbf{4}}$, and αααα-$\ddot{\mathbf{4}}_{out}$, respectively. Such a correlation emphasizes the influence of the repulsion between the chloride anion and the macrocycle on the stereochemistry of the axially coordinated TMCP complexes.

For both HS species, the Cl−Ct distance also significantly decreases by ≈0.1 Å on going from the αααα-$\ddot{\mathbf{3}}_{in}$ or αααα-$\ddot{\mathbf{4}}_{in}$ conformer to the αβαβ conformer. However, the change in the electronic energy is found to be vanishingly small in both cases, thus suggesting that the gain in energy due to the αααα → αβαβ atropisomerization tends to compensate for the destabilization due to the increased repulsion between Cl^- and the macrocycle. This view is actually supported by the results obtained for $\ddot{\mathbf{3}}$ in the LS state. Indeed, upon the HS → LS change of spin states, the Cl−Ct distance decreases by ≈0.4 Å for the two αααα conformers of $\ddot{\mathbf{3}}$ and by ≈0.5 Å for its αβαβ conformers (Table 3). However, while αααα-$\ddot{\mathbf{3}}_{in}$ and αααα-$\ddot{\mathbf{3}}_{out}$ are destabilized by 2044 and 1408 cm^{-1}, respectively, αβαβ-$\ddot{\mathbf{3}}$ is destabilized by 351 cm^{-1} only and becomes the electronically most stable conformer of $\ddot{\mathbf{3}}$ in the LS manifold. That is, the large contraction of the macrocycle upon the HS → LS change of spin states stabilizes the αβαβ conformation with regard to the αααα conformation, and this does more than compensate for the destabilization brought about by the increased repulsion in the αβαβ conformation.

In summary, the RPBE/S' method could be successfully applied to the conformational analysis of the TMCP complexes $\ddot{\mathbf{3}}$ and $\ddot{\mathbf{4}}$. Complex $\ddot{\mathbf{3}}$ is correctly described as a HS species, and good agreement is observed between the optimized and X-ray geometries of the αβαβ conformers of the two HS complexes. The out-of-plane distortion of the porphyrin core proves to be remarkably conserved among the αααα and the αβαβ conformers. The experimentally observed αβαβ conformation is found to be slightly higher in energy than the electronically most stable αααα conformation with the axial Cl^- ligand located on the α side of the macrocycle. This discrepancy can be ascribed to the neglect in our gas-phase conformational analysis of the environmental effects and also to that of the zero-point energy and entropy contributions to the free energies of the isolated conformers. Nonetheless, as demonstrated for $\hat{\mathbf{1}}$, $\hat{\mathbf{2}}$, $\ddot{\mathbf{3}}$, and $\ddot{\mathbf{4}}$, deep insight into the stereochemistry of transition metal complexes of such chiroporphyrins can be obtained through such gas-phase studies.

3.3. The Chloroiron(III) and Chloromanganese(III) BCP8 Complexes. As in the case of the TMCP complexes, the calculations led to the characterization of the conformers of the chloroiron(III) BCP8 complex $\hat{\mathbf{3}}$ in the LS ^2B and the HS ^6A states and to that of the conformers of the chloromanganese(III) BCP8 complex $\hat{\mathbf{4}}$ in the HS ^5A state (see SI).

3.3.1. Structures. Figure 6 shows the optimized HS geometries of the αααα-$\hat{\mathbf{3}}_{in}$, αααα-$\hat{\mathbf{3}}_{out}$, and αβαβ-$\hat{\mathbf{3}}$ conformers.

These geometries resemble their LS counterparts and those of HS $\hat{\mathbf{4}}$ a lot (not shown). For the αααα (respectively, αβαβ) conformers of $\hat{\mathbf{3}}$ and $\hat{\mathbf{4}}$, the predicted structures of the bridled chiroporphyrin exhibit a doming (respectively, ruffling) of the porphyrin macrocycle and ester moieties which have their carbonyl group outwardly (respectively, inwardly) directed. These features are also present in the calculated and the available X-ray structures of the αααα (respectively, αβαβ) conformers of $\hat{\mathbf{1}}$, $\hat{\mathbf{2}}$, $\ddot{\mathbf{3}}$, and $\ddot{\mathbf{4}}$ [1,16,47] as well as in the X-ray geometries of the αααα (respectively, αβαβ) conformer of [MnCl(BCP10)].[2] They are thus predicted to be intrinsic structural features of the αααα (respectively, αβαβ) atropisomers of TMCP and BCP*n* complexes.

Table 6 gives the values of the key structural parameters which help characterize the optimized geometries of the conformers of $\hat{\mathbf{3}}$ and $\hat{\mathbf{4}}$. It also gives the values found for these parameters in the X-ray structures of the αααα and αβαβ conformers of the relevant HS chloromanganese(III) complex of BCP10 [MnCl(BCP10)] ($\hat{\mathbf{5}}$).[2] For the αααα structures of $\hat{\mathbf{3}}$ in either spin state or HS $\hat{\mathbf{4}}$, an inspection shows that, with the exception of the metal atom out-of-plane displacement M−Ct, these parameters which govern the interactions between the MCl fragment (M = Fe, Mn) and the chiroporphyrin tend to adopt in both structures a common set of optimal values. As previously pointed out, the strong sensitivity of the M−Ct parameter to the α or β position of the axial ligand

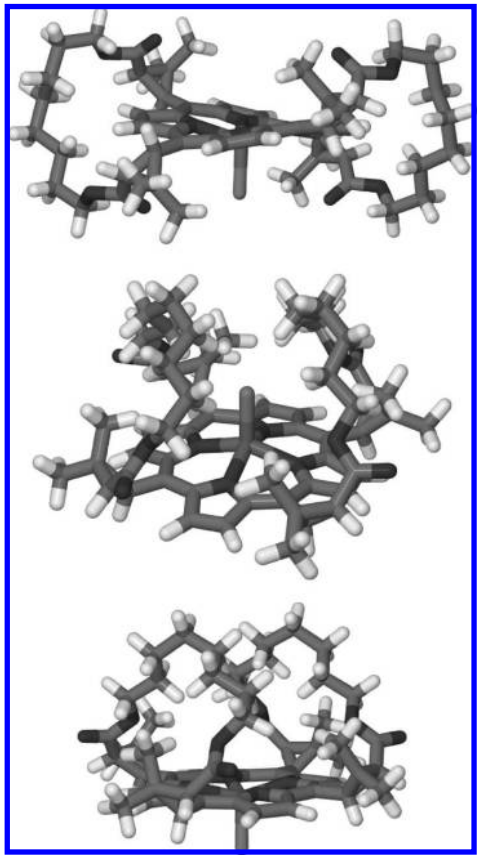

Figure 6. Optimized HS structures of αβαβ-$\hat{\mathbf{3}}$ (top), αααα-$\hat{\mathbf{3}}_{in}$ (middle), and αααα-$\hat{\mathbf{3}}_{out}$ (bottom).

is due to the bonding interaction between the transition metal and Cl atoms, which shifts the metal atom toward the Cl atom. One also notes for $\hat{\mathbf{3}}$ and $\hat{\mathbf{4}}$ in the $\alpha\beta\alpha\beta$ conformation that the metal atom lies out of the macrocycle mean plane (Table 6), in contrast to the in-plane position of the metal atom observed for the $\alpha\beta\alpha\beta$ conformers of $\hat{\mathbf{1}}$ and $\hat{\mathbf{2}}$. The metal atom exhibits a similar out-of-plane displacement for $\ddot{\mathbf{3}}$ and $\ddot{\mathbf{4}}$ in the $\alpha\beta\alpha\beta$ conformation (Table 3). This most probably helps reduce the repulsion between the porphyrin ring and the Cl^- ligand.[58,60]

For discussing the out-of-plane deformations of the macrocycles, we now consider the NSD results summarized in Figure 7 for the optimized geometries of the conformers of $\hat{\mathbf{3}}$ and $\hat{\mathbf{4}}$ in their different spin states, as well as for the experimental geometries of the conformers of HS $\hat{\mathbf{5}}$. For the $\alpha\alpha\alpha\alpha$ conformers of $\hat{\mathbf{3}}$ and $\hat{\mathbf{4}}$, there is a striking conservation of the deformations of the macrocycle, which is predominantly domed with noticeable *ruf* and *sad* deformations (Figure 7). These deformations are similar to those found in the $\alpha\alpha\alpha\alpha$ conformers (*i*) of the BCP8 complexes $\hat{\mathbf{1}}$ and $\hat{\mathbf{2}}$ (Figure 3) but also (*ii*) those of the TMCP complexes $\ddot{\mathbf{3}}$ and $\ddot{\mathbf{4}}$ (Figure 5) and (*iii*) those of the BCP10 complex $\hat{\mathbf{5}}$ (Figure 7). This remarkable conservation of the deformations of the macrocycle is consistent with the observed similarities between the values of Δ_{rms} and $C_\alpha-N-N-C_\alpha$ for the $\alpha\alpha\alpha\alpha$ conformers of all of the considered chiroporphyrin complexes (Tables 1, 3, and 6). It thus follows that the structure of the macrocycle in the $\alpha\alpha\alpha\alpha$ conformation is weakly affected by the presence of the bridles and by their lengths. Remarkably, however, for the chloroiron and chloromanganese complexes in the $\alpha\alpha\alpha\alpha$ conformation characterized by the location of the Cl atom on the α side of the macrocycle, passing from the TMCP to the BCP8 complexes gives rise to a large decrease of the M−Ct distance of about 0.06−0.10 Å and to a shortening of the M−Cl bond of ∼0.02 Å (M = Fe, Mn). Such structural changes are not observed when the Cl atom lies on the β side of the macrocycle (Tables 3 and 6). Therefore, when the Cl atoms and the meso subtituents are in position α, the large shift of the M−Cl fragment toward the macrocycle in passing from the TMCP to the bridled complexes can be ascribed to the steric repulsion between the bridles and the Cl atom.

For the $\alpha\beta\alpha\beta$ conformers of $\hat{\mathbf{3}}$ and $\hat{\mathbf{4}}$, the macrocycle is predominantly ruffled with noticeable displacements along the *sad* and *dom* deformations (Figure 7). These deformations of the macrocycle are well-conserved among these $\alpha\beta\alpha\beta$ conformers. Still, on passing from the iron or manganese TMCP complexes to their BCP8 analogues, there is a drastic decrease of the *ruf* deformation of 0.5 Å at least. This decrease of the *ruf* deformation goes with an increase of the average metal−nitrogen distances of ∼0.02 Å and a decrease of Δ_{rms} and $C_\alpha-N-N-C_\alpha$ by a factor of about two-thirds. This shows that the short bridles are responsible for the porphyrin core being less contracted and less ruffled in complexes of $\alpha\beta\alpha\beta$-BCP8 than in their $\alpha\beta\alpha\beta$-TMCP counterparts. This view is supported by the fact that there is, for $\alpha\beta\alpha\beta$-$\ddot{\mathbf{4}}$ and $\alpha\beta\alpha\beta$-$\hat{\mathbf{5}}$, a better agreement between their structural data than for $\alpha\beta\alpha\beta$-$\hat{\mathbf{4}}$ and $\alpha\beta\alpha\beta$-$\ddot{\mathbf{4}}$. That is, the ruffling of the macrocycle and its concomitant contraction in the $\alpha\beta\alpha\beta$ conformers of the chloromanganese(III) complexes increase in passing from BCP8 to BCP10. This is in line with previous findings on the free base chiroporphyrins $\alpha\beta\alpha\beta$-H_2BCP*n* and on their LS nickel(II) complexes that the restraints imposed on the ruffling of the macrocycle monotonically decrease as the length of the bridles increases from $n = 8$ to $n = 12$.[2]

The influence of the spin state on the structures of the conformers of $\hat{\mathbf{3}}$ proves to be the same as that observed for $\ddot{\mathbf{3}}$. Thus (Table 6), for the three conformers of $\hat{\mathbf{3}}$, the LS → HS change of spin states entails a lengthening of the Fe−N and Fe−Cl bonds of about 0.12 Å and 0.04Å, respectively, which is due to the population of the antibonding $d_{x^2-y^2}$ and d_{z^2} metallic levels. There is also a large increase of the Fe−Ct distance of ∼0.4−0.5 Å, which follows from the interplay between the weakening of the Fe−N bonds and the repulsion between the axial ligand and the macrocycle.[58,60]

Table 6. Metal−Ligand Bond Lengths, out-of-Plane Displacement (M−Ct) of the Metal Atom from the 24-Atom Mean Plane (Å), Root-Mean-Square out-of-Plane Displacement (Δ_{RMS}, in Å) and Ruffling Angle ($C_\alpha-N-N-C_\alpha$) in the Optimized Geometries of the Conformers of the Complexes [FeCl(BCP8)] ($\hat{\mathbf{3}}$) and [MnCl(BCP8)] ($\hat{\mathbf{4}}$)[a]

	spin state	M−N_1	M−N_2	M−N[b]	M−Cl	M−Ct	Δ_{rms}	$C_\alpha-N-N-C_\alpha$
				Optimized Geometries				
$\alpha\alpha\alpha\alpha$-$\hat{\mathbf{3}}_{in}$	HS	2.146	2.125	2.136	2.247	0.727	0.145	3.3
	LS	2.035	2.011	2.023	2.210	0.336	0.115	4.5
$\alpha\alpha\alpha\alpha$-$\hat{\mathbf{3}}_{out}$	HS	2.146	2.126	2.136	2.245	0.438	0.115	3.9
	LS	2.036	2.010	2.023	2.206	0.011	0.127	5.4
$\alpha\beta\alpha\beta$-$\hat{\mathbf{3}}$	HS	2.112	2.142	2.127	2.241	0.652	0.224	22.1
	LS	1.986	2.016	2.001	2.202	0.183	0.243	24.4
$\alpha\alpha\alpha\alpha$-$\hat{\mathbf{4}}_{in}$	HS	2.085	2.057	2.071	2.345	0.492	0.137	3.6
$\alpha\alpha\alpha\alpha$-$\hat{\mathbf{4}}_{out}$	HS	2.083	2.054	2.069	2.343	0.181	0.111	4.5
$\alpha\beta\alpha\beta$-$\hat{\mathbf{4}}$	HS	2.033	2.073	2.053	2.335	0.369	0.235	23.5
				X-Ray Structures				
HS $\alpha\alpha\alpha\alpha$-$\hat{\mathbf{5}}_{in}$[c]	(Mn_2)	2.053, 2.059	2.025, 2.034	2.043	2.365	0.417	0.139	3.9
	(Mn_3)	2.015, 2.036	2.019, 2.019	2.022	2.361	0.428	0.128	5.1
HS $\alpha\beta\alpha\beta$-$\hat{\mathbf{5}}$[c]	(Mn_1)	1.987, 1.994	1.969, 1.983	1.983	2.370	0.363	0.359	35.9

[a] Values found for these parameters in the X-ray structures of the conformers of the relevant complex [MnCl(BCP10)] ($\hat{\mathbf{5}}$) are given for comparison purposes. [b] Average metal−nitrogen distance. [c] The crystal of [MnCl(BCP10)] ($\hat{\mathbf{5}}$; ref 2; Mn_3) and one $\alpha\beta\alpha\beta$ conformer (Mn_1). The molecules have no symmetry, and the distinct M−N_i and M−$N_{i'}$ distances found for each molecule are given.

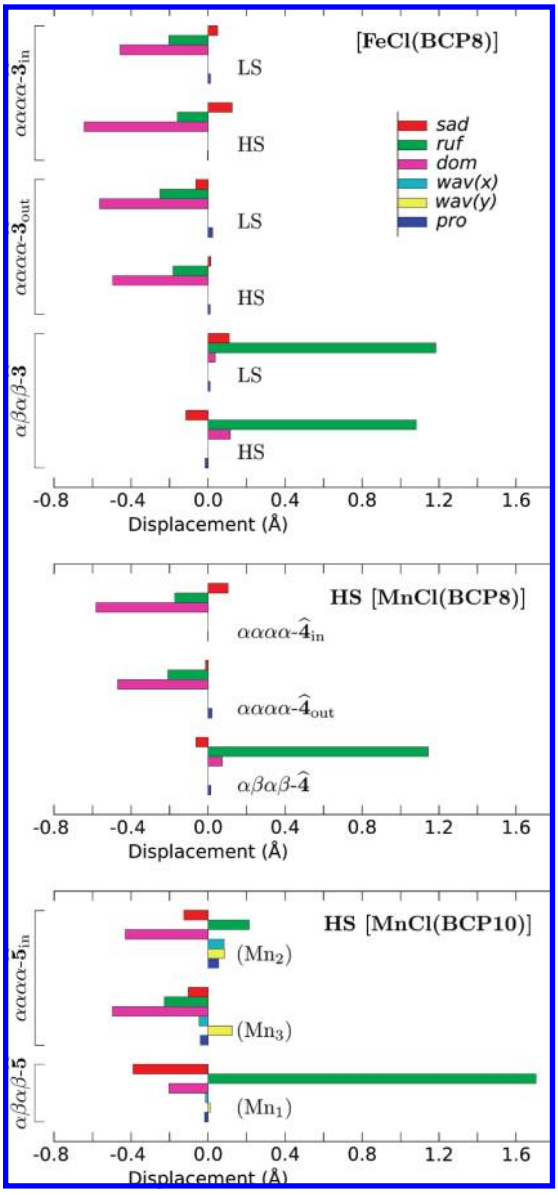

Figure 7. NSD results for the calculated geometries of the conformers of $\hat{\mathbf{3}}$ and $\hat{\mathbf{4}}$. The NSD results obtained for the X-ray structures of the αααα-$\hat{\mathbf{5}}_{in}$ and αααα-$\hat{\mathbf{5}}_{in}$ conformers of $[MnCl(BCP10)]^2$ are also reported.

As compared to $\hat{\mathbf{1}}$ and LS $\hat{\mathbf{2}}$, the porphyrin macrocycle distortion in $\hat{\mathbf{3}}$ and $\hat{\mathbf{4}}$ is actually controlled not only by the occupancy of the stereochemically active $d_{x^2-y^2}$ level but also by the repulsion between the chloride and the porphyrin macrocycle. Thus, on the basis of the occupancy of the antibonding $d_{x^2-y^2}$ level, one would expect that, for any conformation of the BCP8, the metal−nitrogen distances evolve with the nature of the cation and the spin state as follows:

$$Ni^{II}-N \approx Fe^{III}-N|_{LS} \approx Mn^{III}-N|_{HS} < Fe^{III}-N|_{HS} < Zn^{II}-N \quad (5)$$

the rationale behind eq 5 being the fact that the $d_{x^2-y^2}$ level is empty in LS complexes $\hat{\mathbf{2}}$ and $\hat{\mathbf{3}}$ and in HS complex $\hat{\mathbf{4}}$ and that it is singly and doubly occupied in HS $\hat{\mathbf{3}}$ and the $\hat{\mathbf{1}}$ complexes, respectively. However, when one compares the results obtained for the three complexes at the same theoretical levels (Tables 1 and 6), the actual trend proves to be

$$Ni^{II}-N < Fe^{III}-N|_{LS} < Mn^{III}-N|_{HS} \approx Zn^{II}-N < Fe^{III}-N|_{HS} \quad (6)$$

with

$$Fe^{III}-N|_{LS}-Ni^{II}-N \approx 0.02,$$
$$Mn^{III}-N|_{HS}-Ni^{II}-N \approx 0.07,$$
$$Fe^{III}-N|_{HS}-Zn^{III}-N \approx 0.05$$

for the complexes in the αααα conformation and

$$Fe^{III}-N|_{LS}-Ni^{II}-N \approx 0.06,$$
$$Mn^{III}-N|_{HS}-Ni^{II}-N \approx 0.11,$$
$$Fe^{III}-N|_{HS}-Zn^{II}-N \approx 0.08$$

for the complexes in the αβαβ conformation. If the porphyrin core expansion was mainly controlled by the occupancy of the $d_{x^2-y^2}$ level, we would have $Fe^{III}-N|_{LS}-Ni^{II}-N \approx 0 \approx Mn^{III}-N|_{HS} - Ni^{II}-N$ and $Fe^{III}-N|_{HS}-Zn^{II}-N < 0$ (eq 5). Hence, these bond length differences give for $\hat{\mathbf{3}}$ and $\hat{\mathbf{4}}$ a measure of the influence of the axial Cl^- ligand on the porphyrin macrocycle expansion, which it actually favors. Their large increase by passing from the αααα to the αβαβ conformation indicates that the presence of the axial ligand penalizes the contraction of the macrocycle that goes with the αααα → αβαβ atropisomerization. The ruffling which accompanies the atropisomerisation is thus also restrained in $\hat{\mathbf{3}}$ and $\hat{\mathbf{4}}$ by the presence of the axial ligand, the values of Δ_{rms} and $C_\alpha-N-N-C_\alpha$ as well as the *ruf* deformations found for LS and HS αβαβ-$\hat{\mathbf{3}}$ and for HS αβαβ-$\hat{\mathbf{4}}$ remaining significantly lower than those found for αβαβ-$\hat{\mathbf{1}}$ and αβαβ-$\hat{\mathbf{2}}$ (see Tables 1 and 6 and Figures 3 and 7). Inspection of Figures 3 and 7 also shows that there is a large decrease of the *sad* deformations in passing from the RPBE and available X-ray structures of the αβαβ conformers of $\hat{\mathbf{1}}$ and $\hat{\mathbf{2}}$ to those predicted for αβαβ conformers of $\hat{\mathbf{3}}$ and $\hat{\mathbf{4}}$. This suggests that the presence of the axial ligand tends also to prevent the *sad* deformation of the porphyrin core from taking place.

3.3.2. Energetics. The conformational analysis performed for $\hat{\mathbf{3}}$ in the LS and HS states gives the complex as a HS species, as can be inferred from the positive ΔE_{LH} values reported in Table 7. This result is consistent with the one obtained for $\hat{\mathbf{3}}$ and with the fact that the chloroiron(III) porphyrins are HS species.[15,16]

An inspection of Tables 4 and 7 shows that the value of ΔE_{LH} is nearly the same in αααα-$\hat{\mathbf{3}}_{out}$ and αααα-$\ddot{\mathbf{3}}_{out}$, +1426 cm^{-1} versus +1408 cm, whereas it significantly decreases from +2044 cm^{-1} in αααα-$\ddot{\mathbf{3}}_{in}$ to +1307 cm^{-1} in αααα-$\hat{\mathbf{3}}_{in}$. This is evidence that the Cl atom and the bridles directly interact when they are located on the same face of the porphyrin macrocycle, and that these interactions vanish when they are on opposite faces. Furthermore, the decrease of ΔE_{LH} in passing from αααα-$\ddot{\mathbf{3}}_{in}$ to αααα-$\hat{\mathbf{3}}_{in}$ indicates that these interactions destabilize the HS state with regard to the LS state. Given that the

Table 7. Calculated Values of the LS−HS Electronic Energy Difference ΔE_{LH} (cm^{-1}) for the Three Conformers of the Chloroiron(III) BCP8 Complex $\hat{\mathbf{3}}$

αααα-$\hat{\mathbf{3}}_{in}$	αααα-$\hat{\mathbf{3}}_{out}$	αβαβ-$\hat{\mathbf{3}}$
+1307	+1426	+859

Cl atom lies closer to the apex of the cupola made by the bridles in the HS state than in that in the LS state (the Cl−Ct distances in the two spin states differ by about 0.4 Å), the interactions between the Cl atom and the bridles can be identified with the steric repulsion, which was put forth above to explain the systematic ~0.1 Å shift of the Fe−Cl fragment toward the macrocycle observed upon the adjunction of the bridles, on going from αααα-$\ddot{\mathbf{3}}_{in}$ to αααα-$\hat{\mathbf{3}}_{in}$.

One also notes in Table 7 that ΔE_{LH} noticeably decreases to +859 cm^{-1} upon the αααα → αβαβ atropisomerization. This reflects the fact that the large contraction of the macrocycle triggered by the HS → LS change of spin states in $\hat{\mathbf{3}}$ stabilizes the αβαβ conformation. However, the ΔE_{LH} value found for αβαβ-$\hat{\mathbf{3}}$ is larger than the value of +351 cm^{-1} found for αβαβ-$\ddot{\mathbf{3}}$. For αβαβ-$\ddot{\mathbf{3}}$, the vanishing ΔE_{LH} value could be explained by the fact that, upon the HS → LS change of spin states, the stabilization of the αβαβ conformation entailed by the shortening of ~0.1 Å of the Fe−N bonds compensates for the increased repulsion between the chloride ligand and the macrocycle due to the concomitant decrease of the Cl−Ct distance, ~0.5 Å. In αβαβ-$\hat{\mathbf{3}}$, the Fe−N bond lengths and the Cl−Ct distances vary to the same extents as in αβαβ-$\ddot{\mathbf{3}}$. Hence, the lesser stabilization of the αβαβ conformation in $\hat{\mathbf{3}}$ can be ascribed to the presence of the short straps, which restrain the ruffling of the macrocycle.

The HS αααα-$\hat{\mathbf{3}}_{in}$ and αααα-$\hat{\mathbf{4}}_{in}$ conformers are predicted to be the electronically most stable conformers of $\hat{\mathbf{3}}$ and $\hat{\mathbf{4}}$. Table 8 gives the electronic energies of the different conformers of $\hat{\mathbf{3}}$ and $\hat{\mathbf{4}}$ in their different spin states relative to their most stable conformers. For $\hat{\mathbf{3}}$ in either spin state, a same ordering of the energies of the different conformers is observed:

$$\text{αααα-}\hat{\mathbf{3}}_{in} < \text{αααα-}\hat{\mathbf{3}}_{out} < \text{αβαβ-}\hat{\mathbf{3}} \qquad (7)$$

The same inequalities also describe the relative stability of the three conformers of HS $\hat{\mathbf{4}}$:

$$\text{αααα-}\hat{\mathbf{4}}_{in} < \text{αααα-}\hat{\mathbf{4}}_{out} < \text{αβαβ-}\hat{\mathbf{4}} \qquad (8)$$

The comparison of these results with those obtained for the energetics of the conformers of the TMCP complexes (Table 5, eqs 2−4) shows that in all cases the αβαβ form gets strongly destabilized with regard to the αααα forms upon linking the short bridles, which restrict the ruffling of the porphyrin.

The electronic energy differences between the αβαβ conformers and the electronically most stable αααα conformer are +2746 and +2298 cm^{-1} for $\hat{\mathbf{3}}$ in the HS and LS states, respectively, and +3476 cm^{-1} for HS $\hat{\mathbf{4}}$. These energy differences are quite larger than the αβαβ−αααα energy difference of +872 cm^{-1} found for $\hat{\mathbf{2}}$ and compare better with that of +4106 cm^{-1} found for $\hat{\mathbf{1}}$. These observations reflect the fact that the conformers of

Table 8. Calculated Electronic Energies of the Three Conformers of $\hat{\mathbf{3}}$ in the LS and HS States and of the Three Conformers of the HS $\hat{\mathbf{4}}$ Species[a]

αααα-$\hat{\mathbf{3}}_{in}$		αααα-$\hat{\mathbf{3}}_{out}$		αβαβ-$\hat{\mathbf{3}}$	
HS	LS	HS	LS	HS	LS
0	+1307	+649	+2075	+2746	+3605

HS αααα-$\hat{\mathbf{4}}_{in}$	HS αααα-$\hat{\mathbf{4}}_{out}$	HS αβαβ-$\hat{\mathbf{4}}$
0	+1719	+3475

[a] For both complexes, the energy of the most stable form is taken as the zero of the energy scale.

$\hat{\mathbf{3}}$ and $\hat{\mathbf{4}}$ exhibit unexpectedly long metal−nitrogen bonds and that, as found for $\hat{\mathbf{1}}$, an expanded porphyrin core favors the αααα conformation. The axial ligation in $\hat{\mathbf{3}}$ and $\hat{\mathbf{4}}$ is indeed responsible for the metal−nitrogen bonds being relatively long as compared to the Ni−N bonds (even for LS $\hat{\mathbf{3}}$ and HS $\hat{\mathbf{4}}$ with vacant antibonding $d_{x^2-y^2}$ levels), and this in turn limits the extent to which the macrocycle shall ruffle in the αβαβ conformation (see eq 6, and the discussion that follows). Actually, the M−N bonds in $\hat{\mathbf{3}}$ and $\hat{\mathbf{4}}$ are as long as in the TMCP counterparts $\ddot{\mathbf{3}}$ and $\ddot{\mathbf{4}}$. But, although the expanded cores of $\hat{\mathbf{3}}$ and $\hat{\mathbf{4}}$ give αααα-$\ddot{\mathbf{3}}_{in}$ and αααα-$\ddot{\mathbf{4}}_{in}$ as their electronically most stable forms, the calculated αβαβ−αααα energy differences are not as large as in $\hat{\mathbf{3}}$ and $\hat{\mathbf{4}}$. This shows that *both* the long metal−nitrogen bonds induced by the axial ligation and the restraints imposed by the short bridles are actually responsible for the αααα conformation being largely more stable than the αβαβ conformation in $\hat{\mathbf{3}}$ and $\hat{\mathbf{4}}$.

For $\hat{\mathbf{3}}$ and $\hat{\mathbf{4}}$, the destabilization of the αααα conformation on moving the Cl atom from the α to the β face of the macrocycle can be ascribed to the decrease of the Cl−Ct distance by ~0.3 Å and the accompanying increase of the repulsion between the axial ligand and the macrocycle. However, the energy differences between the two αααα conformers are smaller than those found for their TMCP analogues (cf. Tables 5 and 8). Their decrease on going from the TMCP to the BCP8 complexes follows from the steric repulsion between the bridles and the chloride ligand, which destabilizes the αααα conformation with the Cl atom in the α position with regard to the αααα conformation with the Cl atom in the β position.

The results obtained for $\hat{\mathbf{3}}$ in the HS and LS states or for the HS $\hat{\mathbf{4}}$ complex are readily extended to $\hat{\mathbf{3}}$ in the excited intermediate $S = 3/2$ spin state. Indeed, the stereochemistry of $\hat{\mathbf{3}}$ in this spin state and in the LS state should be very similar given that the stereochemically active $d_{x^2-y^2}$ level remains unoccupied in these two spin states and that the lengthening of the Fe−Cl bond on going from the LS to the intermediate spin state should not exceed the ~0.04 Å observed upon the LS → HS change of spin states (for a recent study of the stereochemistry of intermediate-spin iron(III) chiroporphyrins, see ref 61). Consequently, if the intermediate spin state gets admixed into the HS ground state, this will not affect the ground-state stereochemistry of $\hat{\mathbf{3}}$, for which αααα-$\hat{\mathbf{3}}_{in}$ is predicted to be the electronically most stable conformer.

(61) Simonato, J.-P.; Pécaut, J.; Le Pape, L.; Oddou, J.-L.; Jeandey, C.; Shang, M.; Scheidt, W. R.; Wojaczyński, J.; Wołwiec, S.; Latos-Grażyński, L.; Marchon, J.-C. *Inorg. Chem.* **2000**, *39*, 3978–3987.

4. Concluding Remarks

We have carried out a detailed density-functional theory investigation of the stereochemistry of two transition metal complexes of the bridled chiroporphyrin BCP8 and of their bridle-free TMCP analogues, namely, the chloroiron(III) complexes $\hat{\mathbf{3}}$ and $\ddot{\mathbf{3}}$ in the LS and HS states and the HS chloromanganese(III) complexes $\hat{\mathbf{4}}$ and $\ddot{\mathbf{3}}$, thus extending our previous DFT study of the zinc(II) $\hat{\mathbf{1}}$ and LS nickel(II) $\hat{\mathbf{2}}$ BCP8 complexes. The results obtained for the whole set of TMCP and BCP8 complexes allowed us to significantly improve our understanding of the stereochemistry of BCP8 complexes. Specifically, from the exploration of the electronic and structural influences of the transition metal centers on the stereochemistry of the TMCP and BCP8 chiroporphyrins, the following points have been clearly established: (*i*) The complexes in the αααα conformation exhibit a doming of the porphyrin macrocycle which slightly contracts and becomes strongly ruffled upon the αααα → αβαβ atropisomeriszation so as to accommodate the alternating up−down meso substituents. Actually, for the complexes in either conformation, irrespective of the metal center, the BCP8 adopts geometries very similar to one another. (*ii*) The stability of the αααα conformation with respect to the αβαβ conformation markedly increases with the expansion of the porphyrin core for which the metal−nitrogen bond lengths provide a measure. (*iii*) The extent to which the porphyrin macrocycle expands or contracts is determined by the occupancy or vacancy of the stereochemically active $d_{x^2-y^2}$ orbital level but also, in the presence of an axial ligand, by the repulsion between the porphyrin ring and the axial ligand, which tends to favor the expansion of the porphyrin core, hence, the αααα conformation. (*iv*) In the αααα conformation, the repulsion between the axial ligand and the macrocycle favors the location of the axial ligand within the cavity provided by the bridles. (*v*) Due to the restraints this puts on the contraction and ruffling of the macrocycle in the αβαβ conformation, the shortness of the bridles in BCP8 complexes proves to give the right conditions to enable one to strongly discriminate between the αααα and αβαβ conformations on the basis of the expansion of the porphyrin core.

We believe that the stereochemistry of the transition metal complexes of bridled chiroporphyrins can be rationalized on the basis of the above statements, which have been derived from the results of rigorous DFT calculations performed on the BCP8 complexes $\hat{\mathbf{1}}$−$\hat{\mathbf{4}}$ and the TMCP complexes $\ddot{\mathbf{3}}$ and $\ddot{\mathbf{4}}$. The PBE and RPBE results obtained for $\hat{\mathbf{1}}$ and to a much lesser extent for $\hat{\mathbf{2}}$ (Table 2) indicate that the use of different functionals and different basis sets is likely to alter the figures describing the relative electronic stability of the conformers of the investigated complexes. However, the results obtained with the two functionals actually lead to the same conclusions regarding the electronic and structural influences of the Zn(II) and Ni(II) cations on the stereochemistry of the BCP8. We thus believe that the main conlusions (*i*−*v*) drawn from the present study are not sensitive to the choice of the theoretical level used. It is noteworthy that our results show that the use of DFT for investigating the conformational versatility of BCP8 complexes provides a route for the accurate design of molecular switches or nanotweezers wherein the αααα ↔ αβαβ atropisomerization constitutes the primary mechanism. As pointed out in the Introduction, the influences of the zero-point energy, the entropy, and the environment must be taken into account in the DFT calculations for improving their predictive power. Accordingly, we have undertaken a DFT study of the solvated TMCP and BCP8 complexes through the determination of the total free energies of their conformers, while probing further the influence of the choice of the functional and basis set. Preliminary results obtained for $\ddot{\mathbf{3}}$ and $\ddot{\mathbf{4}}$ give the αβαβ conformation as the most stable conformation of the solvated TMCP complexes, in complete agreement with experimental results. These results will be reported soon. Similar work is under way for the BCP8 complexes.

Acknowledgment. We are grateful to W. Robert Scheidt for providing us with the X-ray data of αβαβ-$\ddot{\mathbf{3}}$. We also thank Andreas Hauser and Jacques Pécaut for helpful discussions. L.M.L.D. thanks the Centro Svizzero di Calcolo Scientifico (CSCS) for the calculation resources allocated in the framework of the CSCS project entitled "Photophysics and Photochemistry of Transition Metal Compounds: Theoretical Approaches" and the Swiss National Science Foundation for financial support.

Note Added after ASAP Publication. This article was released ASAP on May 8, 2009, with Greeks throughout the paper in reverse order. The correct version was posted on June 8, 2009.

Supporting Information Available: Mulliken population analyses performed for the electronic states of chloroiron(III) and chloromanganese(III) complexes of the TMCP and BCP8 porphyrins. This material is available free of charge via the Internet at http://pubs.acs.org.